Geochemical Perspectives Letters

In situ determination of NaCl-H_2O isochores up to 900 °C and 1.2 GPa in a hydrothermal diamond anvil-cell

J.K. Li, I-M. Chou, X. Wang

Supplementary Information

The Supplementary Information includes:

- Experimental methods
- Tables S-1 and S-2
- Figures S-1 to S-4
- Supplementary Information References

Experimental methods

Isochores of the H_2O-NaCl system were measured, as illustrated in Figure S-1, by using a Bassett VT-type hydrothermal diamond-anvil cell (HDAC; Li *et al.* 2016), with a newly designed cooling system (Li *et al.* 2020), and a Raman spectrometer. The HDAC sample chamber is a hole (0.5 mm diameter) at the center of the annular rhenium gasket (3 mm diameter and 0.125 mm thick), compressed and sealed by the two parallel diamond anvils (Figure S-2a; Bassett *et al.*, 1993). The sample chamber was heated externally by using two tungsten carbide furnaces, each of which was wrapped with a heating resistance wire. The heating power to the heaters was controlled through a temperature controller (PES1300; Li *et al.* 2020). During cooling, the sample chamber was cooled by a stream of nitrogen, which was cooled through a stainless steel coil immersed in a liquid nitrogen Dewar, as described in Li *et al.* (2020). The temperatures were measured using two K-type thermocouples from Omega Engineering with their tips attached separately to the two diamond anvils. The new thermocouples were calibrated by measuring the triple point of H_2O (0.01 °C), the eutectic point of NaCl solution (-21.2 °C), and the melting points of $NaNO_3$ (306.8 °C) and NaCl (800.5 °C) before experiments, and they were checked again after each experiment to confirm their reliabilities. The reported temperatures are accurate to ± 0.5 °C. A JY/Horiba LabRAM HR Evolution Raman system was used, with an SLWD 20× Olympus objective (0.4 numerical aperture), a 532 nm laser excitation, a grating of 1800-grooves/mm, spectral resolution of 0.2 cm^{-1}, and ~40 mW laser light focused on the sample during the measurement.

At the beginning of each set of isochore experiments, a quartz chip (80 μm thick; as a pressure sensor) from the Jiajika pegmatites, Sichuan, China (Li and Chou, 2016) and H_2O-NaCl solution were loaded and sealed in the sample chamber with a vapour bubble (Figure S-2b). The solutions were prepared with salinities of 2, 5, 10, and 13 wt. % NaCl. Subsequently, considering the new rhenium gasket could be deformed during heating, we heated the sample chamber from ambient to 850 ºC in several cycles until the difference of the two vapor-disappearing (*i.e.*, vapour to liquid homogenization) temperatures (T_hs), in the two adjacent cycles was less than 1 °C to ensure that the sample chamber did have a negligible volume change in the following heating cycle. Such a Re gasket training procedure is the same as that described by Li and Chou (2022).

In the following heating cycle after the Re gasket was trained, we collected the in-situ Raman spectra of quartz in the HDAC sample chamber while the temperature increased from ambient to the temperature above the α-β quartz phase transition temperature (T_{tr}), and the heating rate was reduced from 5 °C/min to 1 °C/min while the temperature was close to T_{tr}. The T_{tr} was determined by the abrupt ~128-cm^{-1} Raman shift of α-quartz as shown in Figure S-1b. At each temperature, the Raman spectrum of quartz, collected for 20–60 s with two accumulations, was repeatedly collected for 3–5 times until the Raman shifts of the 128-cm^{-1} band were constant. Details of this Raman spectroscopic criterion were described by Li and Chou (2022). After a heating cycle, we cooled the sample chamber to the ambient temperature and then repeated the Raman spectra collection procedures during the following heating cycle to check the observed T_{tr}. In the two consecutive heating cycles, we also compared the T_hs to further ensure that the volume of the sample chamber is kept constant. Subsequently, we tightened the driver screws of HDAC to reduce the volume of the sample chamber and thus increase the bulk H_2O-NaCl solution density and then repeated the above experimental procedures to obtain the T_{tr} under a higher pressure condition.

Finally, after the sample chamber was cooled, the final melting temperature of ice (T_{ice}) in the H_2O-NaCl system was measured and the salinity of the fluid in the sample chamber was calculated according to the equation of Bodnar (1993).

Supplementary Tables

Table S-1 Experimental results for the measurements of the isochores of NaCl-H_2O solutions loaded in the sample chamber of a hydrothermal diamond-anvil cell

[a]No.	[b]T_{ice} (°C)	[c]*Sal* (wt. % NaCl)	[d]T_h (°C)	[e]P_h (MPa)	[f]T_{tr} (°C)	[g]P_{tr} (MPa)	[h]P_{trB} (MPa)	[i]P_{trM} (MPa)	[j]P_{trC} (MPa)	[k]P_{error} (%)	[l]Slp_{error} (%)
1	−3.5	5.7	359.7	17.85	638	238.11	223.81	260.76	238.91	0.34	0.36
2	−3.5	5.7	357.1	17.32	643	257.26	232.94	270.61	248.08	3.57	3.83
3	−4.1	6.6	338.0	13.67	661	326.54	298.23	334.94	309.30	5.28	5.51
4	−3.6	5.9	290.0	7.17	705	498.07	471.35	515.12	481.70	3.29	3.33
5	−3.7	6.0	274.4	5.66	719	553.30	540.89	583.61	549.80	0.63	0.64
6	−3.7	6.0	271.4	5.40	722	565.17	555.04	597.43	563.72	0.26	0.26
7	−3.7	6.0	258.0	4.35	739	632.74	625.34	665.57	633.06	0.05	0.05
8	−3.7	6.0	247.9	3.67	754	692.74	684.25	721.70	691.26	0.21	0.21
9	−3.7	6.0	239.4	3.17	765	736.96	733.72	767.66	740.12	0.43	0.43
10	−4.3	6.9	210.2	1.82	802	887.15	925.70	935.80	924.50	4.21	4.22
11	−4.6	7.3	200.0	1.47	829	998.14	1024.31	1019.97	1016.97	1.89	1.89
12	−4.3	6.9	263.0	4.69	740	636.72	613.98	654.84	620.47	2.55	2.57
13	−4.6	7.3	287.5	6.84	709	513.82	493.89	535.38	501.59	2.38	2.41
14	−9.0	12.8	442.0	37.28	609	127.82	141.35	138.99	134.31	5.08	7.18
15	−6.7	10.1	394.8	25.13	621	173.29	187.11	198.79	186.29	7.50	8.78
16	−9.0	12.8	391.4	23.70	633	219.00	215.14	222.93	213.89	2.33	2.62
17	−9.0	12.8	377.8	20.62	634	222.82	236.89	248.00	237.27	6.49	7.15
18	−6.4	9.7	366.4	18.69	647	272.61	250.04	270.44	252.72	7.30	7.83
19	−10.4	14.4	365.1	17.73	648	276.45	278.78	291.72	281.30	1.75	1.88
20	−9.2	13.1	355.0	15.99	656	307.24	299.24	316.66	301.70	1.80	1.90
21	−10.4	14.4	345.0	14.04	669	357.50	340.46	358.89	343.70	3.86	4.02
22	−10.4	14.4	325.1	10.93	690	439.24	411.41	434.41	413.62	5.83	5.98
23	−10.8	14.8	312.0	9.14	706	502.00	469.24	493.48	469.18	6.54	6.66
24	−10.4	14.4	311.0	9.04	707	505.94	470.39	495.69	470.45	7.02	7.14
25	−9.8	13.7	272.0	5.12	752	684.71	655.66	680.62	643.26	6.05	6.10
26	−8.9	12.7	260.0	4.27	761	720.86	706.60	730.73	691.56	4.06	4.09
27	−9.2	13.1	211.8	1.79	803	891.24	1004.69	983.63	947.77	6.34	6.35
28	−9.2	13.1	203.2	1.51	819	956.90	1079.95	1044.71	1011.82	5.74	5.75
29	−8.4	12.2	200.0	1.42	824	977.50	1092.46	1057.04	1030.35	5.41	5.42
30	−8.6	12.4	272.0	5.18	740	636.72	627.20	655.88	619.28	2.74	2.76
31	−7.7	11.3	186.8	1.08	837	1031.24	1178.32	1122.40	1111.04	7.74	7.75
32	−12.0	16.0	432.7	33.28	620	173.29	167.83	169.95	164.86	4.86	6.02
33	−12.5	16.4	428.0	31.83	625	188.50	177.11	184.26	176.14	6.56	7.89
34	−11.7	15.7	394.0	23.65	632	215.18	222.62	227.04	224.11	4.15	4.66
35	−11.7	15.7	349.6	14.66	665	342.00	333.62	348.90	337.54	1.30	1.36

36	−11.7	15.7	335.5	12.34	680	400.23	382.20	400.67	385.40	3.70	3.82
37	−13.8	17.6	304.6	8.02	709	513.82	517.00	534.26	512.37	0.28	0.29
38	−14.1	17.9	283.3	5.85	744	652.70	639.34	654.28	623.08	4.54	4.58
39	−11.9	15.9	196.0	1.26	838	1035.39	1199.83	1136.90	1090.06	5.28	5.29
40	−12.5	16.4	187.0	1.04	846	1068.61	1280.51	1196.92	1148.28	7.46	7.46
41	−12.5	16.4	199.0	1.34	839	1039.54	1191.24	1132.31	1081.03	3.99	4.00
42	−11.9	15.9	180.0	0.89	860	1127.00	1345.65	1245.30	1203.58	6.80	6.80
43	−16.6	19.9	413.0	26.84	628	199.92	210.48	206.56	217.03	8.56	9.88
44	−17.0	20.2	393.0	22.25	644	261.10	255.66	254.24	263.68	0.99	1.08
45	−17.0	20.2	378.0	19.15	655	303.39	292.20	293.38	300.45	0.97	1.03
46	−18.3	21.2	334.0	11.43	686	423.62	430.64	435.95	434.01	2.45	2.52
47	−18.3	21.2	300.0	7.22	725	577.06	582.20	589.64	572.05	0.87	0.88
48	−18.0	21.0	288.0	6.08	740	636.72	643.44	650.73	625.94	1.69	1.71
49	−17.4	20.5	240.4	2.84	790	838.20	920.29	910.66	856.45	2.18	2.18
50	−17.4	20.5	220.8	1.98	815	940.44	1065.59	1038.90	972.15	3.37	3.38
51	−17.4	20.5	196.8	1.23	849	1081.10	1270.38	1211.77	1130.43	4.56	4.57
52	−16.2	19.6	229.2	2.34	813	932.23	1007.95	988.78	929.32	0.31	0.31
53	−16.2	19.6	237.0	2.70	807	907.62	957.09	944.96	889.38	2.01	2.02
Average value										3.69	3.90

Note:

[a]No.: experimental number;

[b]T_{ice}: ice point of NaCl-H_2O solution measured in HDAC with the cooling system after the Raman spectroscopic measurements of the α-β quartz phase transition;

[c]*Sal*: salinity of NaCl-H_2O solution calculated from Bodnar (1993);

[d]T_h: vapor bubble-disappearing temperature in the HDAC sample chamber;

[e]P_h: pressure at T_h calculated with the equation of Bodnar (1983);

[f]T_{tr}: the measured α-β quartz phase transition temperature;

[g]P_{tr}: the sample pressure at T_{tr} calculated according to the refined α-β quartz *P–T* boundary of Li and Chou (2022);

[h]P_{trB}: the sample pressure at T_{tr} calculated from the NaCl-H_2O isochore of Bodnar and Vityk (1994);

[i]P_{trM}: the sample pressure at T_{tr} calculated from the NaCl-H_2O isochore of Mao *et al.* (2015);

[j]P_{trC}: the sample pressure at T_{tr} calculated from the fitted Equations (1) shown in the text;

[k]P_{error}: the error between [g]P_{tr} and [j]P_{trC}. [k]$P_{error} = |{}^{g}P_{tr} - {}^{j}P_{trC}| / {}^{g}P_{tr} \times 100\%$.

[i]Slp_{error}: the slope errors between measured isochores ($Isochore_M$s) and fitted isochores ($Isochore_F$s), which were determined with [(T_h, P_h), (T_{tr}, P_{tr})] and [(T_h, P_h), (T_{tr}, P_{trc})], respectively. [i]$Slp_{error} = |Isochore_M - Isochore_F| / Isochore_M \times 100\%$.

Table S-2 Pressures at specified temperatures along the isochores of NaCl-H_2O solutions interpolated from the listed values of Hurai (1988)

[a]T_h (°C)	[b]Temperature (°C) on the isochore														
	150 °C	175	200	225	250	275	300	325	350	375	400	425	450	475	500
	[c]Pressure (MPa) on the isochore														
5 wt. % NaCl															
150	[c]40 ([d]−3.4)	437 (−1.0)	87.7 (0.7)	132.4 (1.7)	177.8 (1.9)	223.6 (1.8)	270.0 (1.1)	316.3 (0.4)	362.7 (−0.3)	408.8 (−0.7)	454.7 (−0.9)	500.7 (−1.3)	[e]\	\	\
200			1.5 (−1.3)	41.5 (−0.4)	81.4 (0.4)	122.0 (0.5)	162.8 (0.6)	204.0 (0.1)	244.0 (0.9)	284.8 (0.8)	326.0 (0.4)	367.9 (−0.7)	408.7 (−0.8)	449.2 (−0.6)	489.1 (0.3)
250					3.9 (−1.6)	37.5 (−0.2)	710 (1.2)	105.7 (1.5)	141.4 (0.7)	177.1 (0.0)	212.6 (−0.6)	247.7 (−0.7)	282.7 (−0.7)	317.2 (−0.3)	351.0 (0.8)
300							8.3 (−1.7)	34.1 (0.1)	61.4 (0.4)	88.9 (0.4)	116.6 (0.3)	144.3 (0.2)	172.4 (−0.3)	200.3 (−0.6)	228.2 (−0.9)
9 wt. % NaCl															
150	−25	44.3 (−0.9)	89.0 (0.4)	133.9 (1.3)	179.5 (1.7)	226.3 (0.8)	271.6 (1.4)	317.9 (1.0)	364.5 (0.3)	411.0 (−0.3)	457.6 (−1.0)	504.3 (−1.8)	\	\	\
200			1.5 (−0.9)	41.8 (−0.1)	83.0 (−0.3)	126.4 (−2.5)	163.9 (1.0)	205.1 (0.9)	244.9 (2.2)	286.2 (2.0)	328.0 (1.2)	370.8 (−0.5)	412.3 (−0.9)	453.8 (−1.4)	494.2 (−0.7)
250					3.7 (−2.1)	37.5 (−0.1)	71.4 (1.7)	107.0 (1.8)	143.8 (0.7)	180.3 (−0.1)	216.8 (−0.9)	2527. (−1.1)	288.4 (−1.1)	323.1 (−0.1)	357.5 (1.2)
300							8.1 (−2.0)	34.9 (0.5)	63.9 (0.7)	93.0 (0.9)	122.5 (0.6)	151.8 (0.5)	181.7 (−0.2)	211.2 (−0.4)	240.8 (−0.8)
13 wt. % NaCl															
150	4 (−27)	44.8 (−0.8)	90.0 (0.2)	135.3 (1.2)	181.2 (1.5)	227.1 (1.8)	274.0 (1.2)	320.6 (0.8)	367.7 (−0.1)	414.9 (−1.0)	462.1 (−2.0)	\	\	\	\
200			1.4 (−2.4)	41.9 (−1.2)	82.5 (0.0)	123.8 (0.4)	165.2 (0.8)	206.6 (1.1)	247.1 (2.3)	289.2 (2.0)	331.5 (1.4)	375.1 (−0.5)	417.3 (−1.0)	459.8 (−1.7)	501.1 (−1.3)
250					3.6 (−2.3)	37.9 (−0.1)	72.5 (1.9)	109.1 (1.8)	146.7 (0.8)	184.1 (0.0)	221.5 (−0.9)	258.3 (−1.1)	295.0 (−1.2)	330.4 (−0.1)	365.8 (1.1)
300							7.8 (−1.7)	36.6 (0.4)	67.3 (0.6)	98.1 (0.7)	129.2 (0.5)	160.2 (0.4)	191.7 (−0.2)	222.7 (−0.3)	254.0 (−0.7)
17 wt. % NaCl															
150	4	45.2	90.9	136.7	183.1	229.5	276.9	324.5	372.4	420.3	468.2	\	\	\	\

	(−30)	(−0.9)	(0.2)	(1.2)	(1.7)	(2.2)	(1.6)	(0.9)	(−0.2)	(−1.2)	(−2.3)				
200			1.4 (−3.1)	41.9 (−1.3)	82.8 (0.3)	124.7 (0.7)	166.6 (1.3)	207.8 (2.5)	250.7 (2.0)	293.4 (1.7)	336.7 (0.8)	380.8 (−0.9)	423.8 (−1.5)	467.2 (−2.6)	506.7 (0.3)
250					3.6 (−2.3)	37.9 (−0.1)	72.5 (1.9)	109.1 (1.8)	146.7 (0.8)	184.1 (0.0)	221.5 (−0.9)	258.3 (−1.1)	295.0 (−1.2)	330.4 (−0.1)	365.8 (1.1)
300							7.5 (−0.8)	39.2 (0.2)	71.5 (0.4)	104.2 (0.2)	136.8 (0.2)	169.4 (0.2)	202.3 (−0.1)	234.9 (−0.2)	267.6 (−0.3)
21 wt. % NaCl															
150	4 (−39)	45.3 (−1.1)	91.5 (0.4)	138.0 (1.6)	185.2 (2.0)	232.2 (2.7)	280.5 (2.1)	329.4 (0.9)	378.3 (−0.4)	427.3 (−1.7)	475.9 (−2.6)	\	\	\	\
200			1.3 (−4.4)	41.6 (−1.3)	82.9 (0.8)	125.7 (1.3)	168.1 (2.2)	210.4 (3.3)	255.6 (1.4)	299.2 (1.1)	343.5 (0.2)	387.8 (−0.8)	431.7 (−1.4)	476.0 (−2.4)	\
250					3.3 (−2.6)	39.7 (−0.3)	77.2 (0.8)	115.8 (0.8)	153.5 (1.8)	192.7 (1.3)	232.0 (0.5)	271.3 (−0.1)	310.5 (−0.7)	349.2 (−0.7)	3878 (−0.7)
300							72. (0.8)	42.7 (−0.4)	76.6 (−0.1)	111.3 (−0.5)	145.3 (−0.2)	179.4 (0.0)	213.6 (0.0)	247.8 (0.1)	281.8 (0.3)
25 wt. % NaCl															
150	4 (−51)	45.3 (−1.3)	91.9 (0.7)	139.2 (2.2)	187.4 (2.7)	235.4 (3.4)	284.9 (2.6)	335.3 (0.9)	385.6 (−0.7)	435.9 (−2.3)	485.2 (−2.9)	\	\	\	
200			1.2 (−5.9)	41.1 (−1.3)	82.8 (1.4)	126.6 (2.1)	169.7 (3.4)	212.7 (4.9)	261.8 (0.2)	306.5 (0.0)	351.9 (−1.0)	396.2 (−0.8)	441.1 (−1.2)	486.2 (−1.9)	\
250					3.2 (−2.5)	41.1 (−0.6)	80.8 (−0.4)	120.4 (−0.1)	157.6 (2.5)	197.5 (24)	238.0 (1.8)	278.8 (0.8)	319.5 (0.0)	360.7 (−1.3)	401.5 (−2.3)
300							6.9 (3.0)	47.0 (−1.1)	82.6 (−0.7)	119.5 (−1.6)	154.6 (−0.8)	190.2 (−0.4)	225.6 (0.2)	261.3 (0.4)	2966 (1.1)

[a] T_h, liquid-vapor homogenization (to liquid phase) temperature.

[b] specified temperature on the isochore of NaCl-H_2O solution.

[c] pressure, interpolated from the listed values in Hurai (1988), at the specified temperature on the isochore corresponding to the T_h.

[d] deviation of the pressure, calculated with the linear equation that fitted the P–T data of the isochore corresponding to the T_h, from the [c] pressure.

[e] not available; the data of Hurai (1988) are below ~500 MPa.

Supplementary Figures

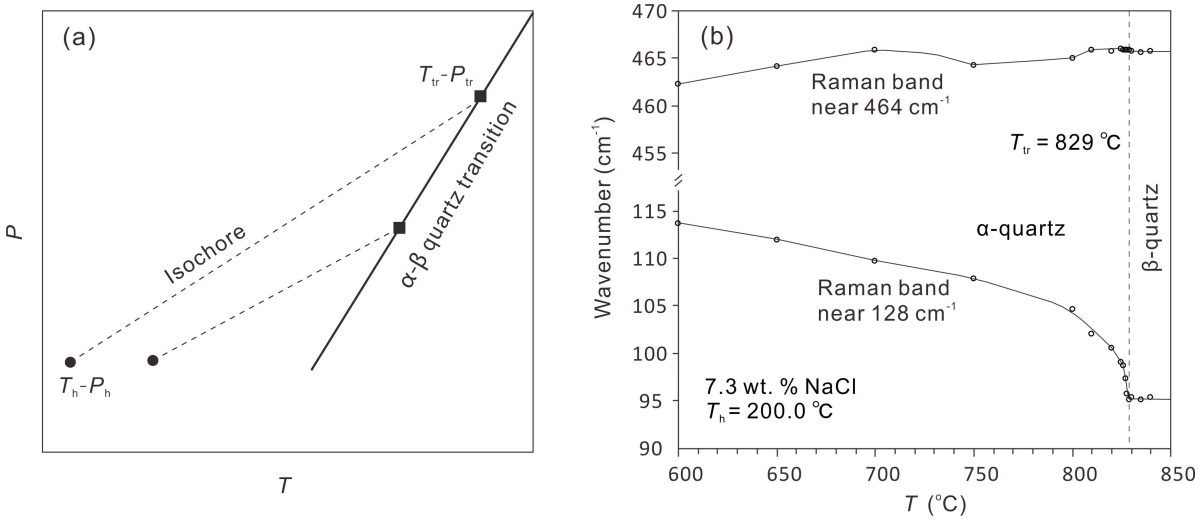

Figure S-1 (a) Diagram showing the isochores (dashed lines) of the fluid inside the HDAC sample chamber determined by α-β quartz transition temperature (T_{tr}) –pressure (P_{tr}) boundary (squares on the solid α-β quartz phase transition line) and the L–V homogenization temperature (to L; T_h) –pressure (P_h) (dots). **(b)** Diagram illustrating the advantage of using the Raman shift of the quartz band near 128 cm^{-1} relative to 464 cm^{-1} for the determination of the T_{tr}, during heating, for an NaCl-H_2O solution (with salinity of 7.3 wt. % NaCl and T_h of 200 °C) loaded in the HDAC sample chamber; plotted are the data from Exp. 11 listed in Table S-1, and T_{tr} at 829 °C is marked by the vertical dashed line. The two solid lines show the trends of the temperature dependence of the Raman shifts for the 128 (lower) and 464-cm^{-1} (upper) quartz bands in both α- and β-quartz.

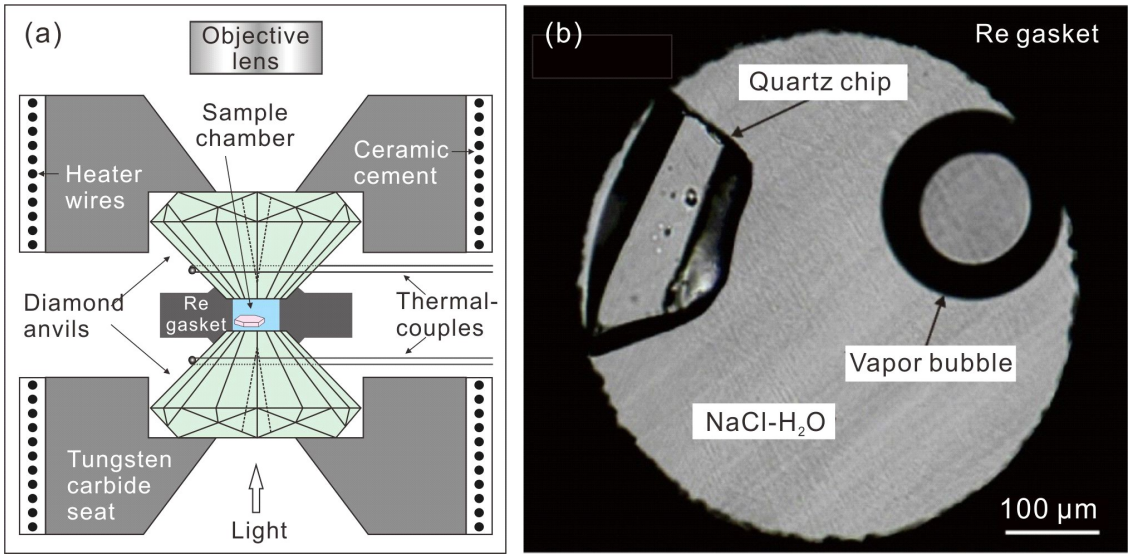

Figure S-2 (a) A schematic diagram of the central portion of a hydrothermal diamond-anvil cell (HDAC) and **(b)** the sample chamber loaded with quartz wafer and NaCl-H_2O solution (after Bassett *et al.*, 1993; *Li et al.*, 2016)

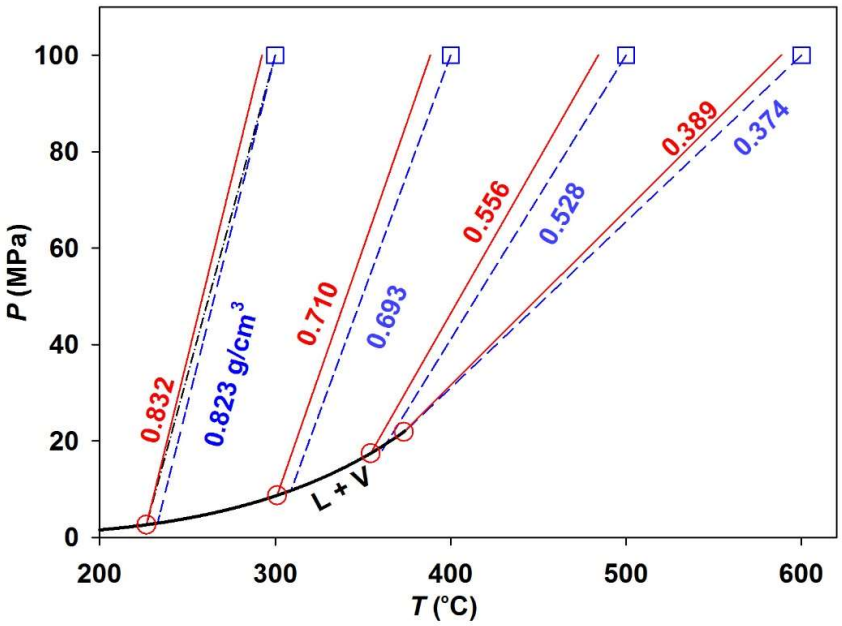

Figure S-3 *P*–*T* (isoplethal) projection showing isochores (g/cm^3) of pure H_2O derived from the synthetic fluid inclusion technique data (Bodnar and Sterner, 1987, their Table 17.1) for inclusions formed under 100 MPa. The four blue open squares are the formation *P*–*T* points (at 100 MPa and 300, 400, 500 and 600 ºC) of fluid inclusions in quartz, and the corresponding isochores derived from the NIST Table (Wagner and Pruß, 2002) are shown by the dashed blue lines, which end at the liquid-vapor curve (solid black line). The four open red circles on the liquid-vapor curve are the corresponding average liquid-vapor homogenization (to liquid) *P*–*T* points of fluid inclusions, and their corresponding isochores are shown by the solid red lines. It is clearly shown that the density represented by the isochoric red line is always higher than that of the corresponding dashed blue line, and that the lines connecting the open red circle and the corresponding blue square (*e.g.,* the black dash-dot line for inclusions formed at 100 MPa and 300 ºC) are not isochoric.

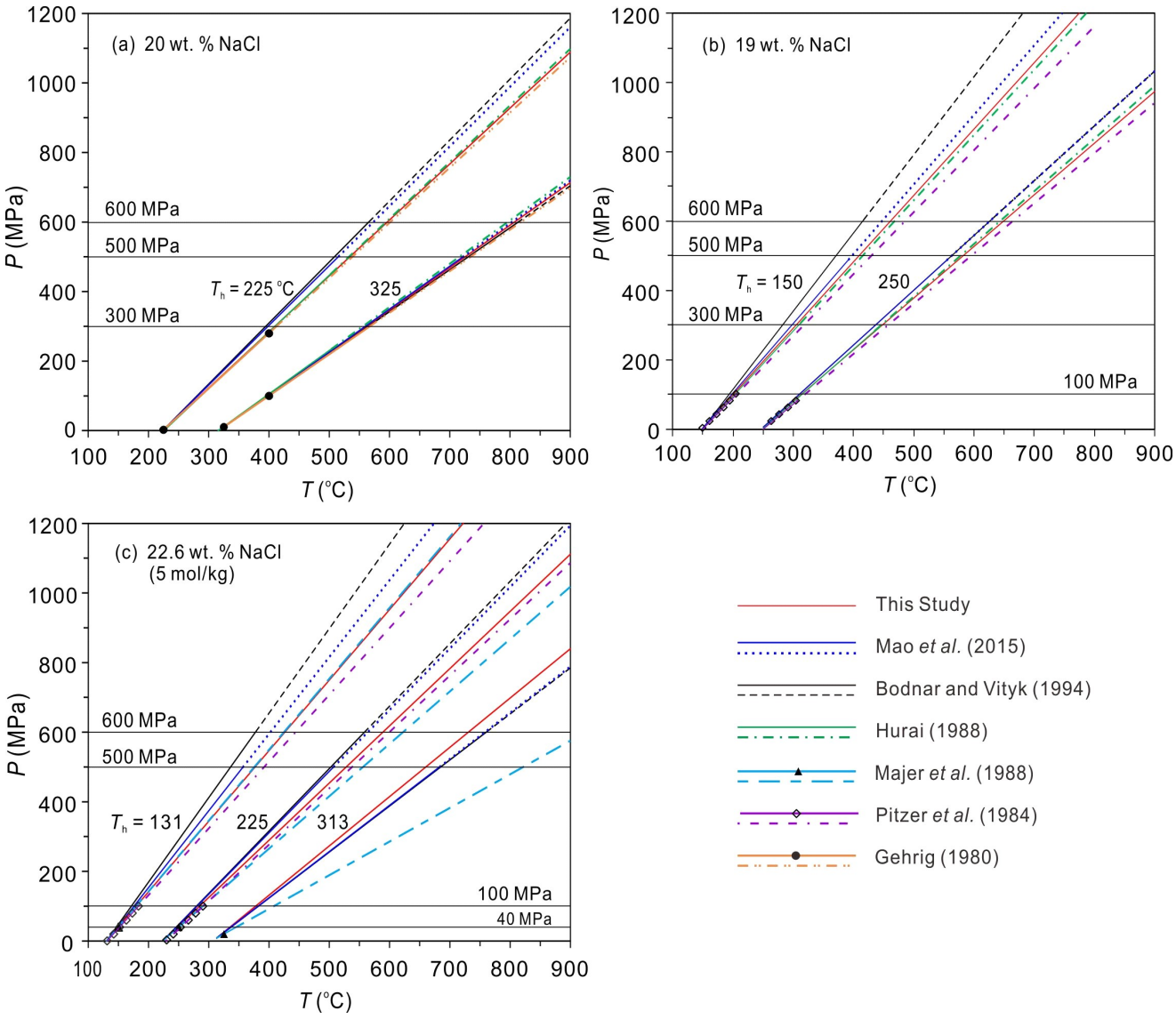

Figure S-4 Comparisons of NaCl-H_2O isochores derived from our data (red lines) and previous ones with **(a)** 20 wt. % NaCl, **(b)** 19 wt. % NaCl, and **(c)** 22.6 wt. % NaCl. The previous isochores include those from Bodnar and Vityk (1994; applicable at ≤600 MPa), Mao *et al.* (2015; applicable at ≤500 MPa), and those linearly fitted with the data in tables of Majer *et al.* (1988; triangle, applicable at ≤40 MPa), Hurai (1988; applicable at ≤500 MPa and 500 °C), Pitzer *et al.* (1984; diamond, applicable at ≤100 MPa), and Gehrig (1980; circle, applicable at ≤300 MPa). All data are represented by solid lines, and extrapolations are shown by other line symbols as indicated in the figure legends at the lower right corner. The homogenization temperatures (T_hs) are marked.

Supplementary Information References

Bassett, W.A., Shen, A.H., Bucknum, M., Chou, I−M. (1993) A new diamond anvil cell for hydrothermal studies to 2.5 GPa and from –190 to 1200 °C. *Review of scientific instruments* 64, 2340–2345. https://doi.org/10.1063/1.1143931

Bodnar, R.J. (1983) A method of calculating fluid inclusion volumes based on vapor bubble diameters and *P-V-T-X* properties of inclusion fluids. *Economic Geology* 78, 535–542. https://doi.org/10.2113/gsecongeo.78.3.535

Bodnar, R.J. (1993) Revised equation and table for determining the freezing point depression of NaCl-H_2O solutions. *Geochimica et Cosmochimica Acta* 57, 683–684. https://doi.org/10.1016/0016-7037(93)90378-A

Bodnar, R.J., Sterner, S.M. (1987) Synthetic fluid inclusions. In: Ulmer, G.C., Barnes, H.L. (Eds.) *Hydrothermal Experimental Techniques*, Wiley-Interscience, New York. 423–457.

Bodnar, R.J., Vityk, M.O. (1994) Interpretation of Microthermometric data for H_2O-NaCl fluid inclusions. In: Vivo, B.D., Frezzoti, M.L. (Eds.) *Fluid Inclusions in Minerals: Methods and Applications*. Virginia Tech., Blacksburg, VA. 117–130.

Hurai, V. (1988) *P–V–T–X* tables of water and 1–25 weight percent NaCl-H_2O solutions to 500 °C and 500 × 10^5 Pa. *Acta Geologica et Geographica Universitatis Comenianae* 44, 101–135.

Gerhig, M. (1980) Phasengleichgewichte und PVT-Daten temiirer Mischungen aus Wasser, Kohlendioxid und Natriumchlorid bis 3 kbar und 550°C. Ph.D. dissertation, Universitat Karlsruhe, 109p.

Li, J.K., Chou, I-M. (2016) An occurrence of metastable cristobalite in spodumene-hosted crystal-rich inclusions from Jiajika pegmatite deposit, China. *Journal of Geochemical Exploration* 171, 29–36. https://doi.org/10.1016/j.gexplo.2015.10.012

Li, J.K., Bassett, W.A., Chou, I-M, Ding, X., Li, S.H, Wang, X.Y. (2016) An improved hydrothermal diamond anvil cell. *Review of Scientific Instruments* 87, 053108. https://doi.org/10.1063/1.4947506

Li, J.K., Chou, I. M., Bassett, W.A., Wang, X. (2020) A new type of hydrothermal diamond-anvil cell with cooling system. *Review of Scientific Instruments* 91, 053104. https://doi.org/10.1063/1.5143596

Li, S.H., Chou, I-M. (2022) Refinement of the α-β quartz phase boundary based on in situ Raman spectroscopy measurements in hydrothermal diamond-anvil cell and an evaluated equation of state of pure H_2O. *Journal of Raman Spectroscopy* 53, 1471-1482. https://doi.org/10.1002/jrs.6367

Majer, V., Gates, J.A., Inglese, A., Wood, R.H. (1988) Volumetric properties of aqueous NaCl solutions from 0.0025 to 5.0 mol kg1, 323 to 600 K, and 0.1 to 40 MPa. *The Journal of Chemical Thermodynamics* 20, 949–968. https://doi.org/10.1016/0021-9614(88)90224-8.

Mao, S., Hu, J., Zhang, Y., Meng, X.L. (2015) A predictive model for the PVTX properties of CO_2–H_2O–NaCl fluid mixture up to high temperature and high pressure. *Applied Geochemistry* 54, 54–64. https://doi.org/10.1016/j.apgeochem.2015.01.003

Pitzer, K.S., Peiper, J.C., Busey, R.H. (1984) Thermodynamic properties of aqueous sodium chloride solutions. *Journal of Physical and Chemical Reference Data* 13, 1–102. https://doi.org/10.1021/ja01341a002

Wagner, W., Pruβ, A. (2002) The IAPWS formulation 1995 for the thermodynamic properties of ordinary water substance for general and scientific use. *Journal of Physical and Chemical Reference Data* 31, 387–535. https://doi.org/10.1063/1.1461829